BBA - Biomembranes 1860 (2018) 737–748

Contents lists available at ScienceDirect

BBA - Biomembranes

journal homepage: www.elsevier.com/locate/bbamem

Effect of N-terminal acetylation on lytic activity and lipid-packing perturbation induced in model membranes by a mastoparan-like peptide

Dayane S. Alvares[a], Natalia Wilke[b], João Ruggiero Neto[a,*]

[a] UNESP - São Paulo State University, IBILCE, Department of Physics, São José do Rio Preto, SP, Brazil
[b] Centro de Investigaciones en Química Biológica de Córdoba (CIQUIBIC-CONICET), Departamento de Química Biológica, Facultad de Ciencias Químicas, Universidade Nacional de Córdoba, Argentina

ARTICLE INFO

Keywords:
Membrane perturbation
Acetylated peptide
GUVs
CD
Lipid monolayer
Fluorescence microscopy
DSC

ABSTRACT

L1A (IDGLKAIWKKVADLLKNT-NH2) is a peptide that displays a selective antibacterial activity to Gram-negative bacteria without being hemolytic. Its lytic activity in anionic lipid vesicles was strongly enhanced when its N-terminus was acetylated (ac-L1A). This modification seems to favor the perturbation of the lipid core of the bilayer by the peptide, resulting in higher membrane lysis. In the present study, we used lipid monolayers and bilayers as membrane model systems to explore the impact of acetylation on the L1A lytic activity and its correlation with lipid-packing perturbation. The lytic activity investigated in giant unilamellar vesicles (GUVs) revealed that the acetylated peptide permeated the membrane at higher rates compared with L1A, and modified the membrane's mechanical properties, promoting shape changes. The peptide secondary structure and the changes in the environment of the tryptophan upon adsorption to large unilamellar vesicles (LUVs) were monitored by circular dichroism (CD) and red-edge excitation shift experiments (REES), respectively. These experiments showed that the N-terminus acetylation has an important effect on both, peptide secondary structure and peptide insertion into the bilayer. This was also confirmed by experiments of insertion into lipid monolayers. Compression isotherms for peptide/lipid mixed films revealed that ac-L1A dragged lipid molecules to the more disordered phase, generating a more favorable environment and preventing the lipid molecules from forming stiff films. Enthalpy changes in the main phase transition of the lipid membrane upon peptide insertion suggested that the acetylated peptide induced higher impact than the non-acetylated one on the thermotropic behavior of anionic vesicles.

1. Introduction

Lytic peptides with bactericidal activity have been extensively investigated over the past few decades due to the emergence of resistant bacteria [1,2]. The action mechanisms of these peptides have been extensively reviewed [3,4] but are not completely understood. In all the proposed mechanisms, the peptide first adsorbs onto the membrane surface. The large number of their cationic and hydrophobic residues favors their folding to amphipathic helical or beta structures when they are in contact with lipid membranes [1,5]. This coupled partition and folding process is mainly driven by electrostatic and hydrophobic energetic contributions. In the case of helical peptide, the hydrophilic face is in contact with the lipid polar head groups, while the hydrophobic face is in contact with the lipidic phase of the bilayer [6]. The stiffness of the peptide imposes deformations in the flexible acyl chains, creating elastic stress in the bilayer that is relieved by the onset of lytic activity. In the electrostatic-hydrophobic balance involved in these initial steps, a correlation has been observed between net charge, affinity and lytic activity in anionic lipid vesicles [6–8].

Although the peptide net charge modulates its affinity for lipid vesicles through electrostatic interactions, this factor does not alway ensure lytic efficiency. Evidence has shown that the peptide capability of insertion into the hydrophobic region of the lipid membrane can lead to more productive lytic activity. The insertion of some peptides into lipid membranes is hampered by the dipole distribution of the lipid bilayer when the insertion is made by their N-terminus [9]. Experimental evidence of the interaction of somatostatin with POPC bilayers [10] (also confirmed by molecular dynamics simulations [11]) revealed that the positive charge on the N-terminal is the first energy barrier to peptide insertion into the bilayer, and thus, the reduction of the N-terminus charge leads to a lower energy barrier to its insertion. As a result, the deprotonation of the N-terminus allows the peptide to be inserted more deeply into the bilayer core, and, consequently, induces higher perturbation in the lipid-packing. This seems to be the case of

* Corresponding author.
E-mail address: jruggiero@sjrp.unesp.br (J. Ruggiero Neto).

https://doi.org/10.1016/j.bbamem.2017.12.018
Received 23 June 2017; Received in revised form 4 December 2017; Accepted 20 December 2017
Available online 26 December 2017

the synthetic peptide L1A (IDGLKAIWKKVADLLKNT-NH_2). This peptide has a selective bactericidal activity against Gram-negative bacteria and is non-hemolytic, displaying a strong and quick lytic activity in anionic lipid vesicles [12]. The neutralization of the N-terminus positive charge by acetylation (ac-L1A) significantly enhanced its lytic activity in mixed anionic vesicles [13]. Acetylation was observed to increase its helical content and the tryptophan blue-shift and, when in vesicles, this residue was more screened from its quencher acrylamide, suggesting that this simple modification resulted in a deeper insertion of the peptide into the hydrophobic region of the bilayer. In addition, this modification did not influence its affinity for anionic vesicles as determined by the partition constants [13], despite the lower net charge. These observations suggest that the perturbation induced in the bilayer was more productive in increasing its lytic action. These results also suggest that the initial steps involving peptide adsorption onto the membrane surface and its folding and insertion into the lipid bilayer modulate its lytic activity. The comprehension of these initial steps is therefore of paramount importance.

To obtain an insight into how L1A and its acetylated analog disturb lipid-packing we used monolayers and bilayers of phosphatidylcholine (PC), which mimic the lipid composition of mammalian membranes (outer leaflet essentially zwitterionic, with predominance of PC), and PC with phosphatidylglycerol (PG), which mimic the plasma bacterial membrane of Gram-negative bacteria (containing ~20% of anionic lipid, mostly PG in the outer membrane [14]). The lytic activity of these peptides was assessed in giant unilamellar vesicles (GUVs) and in large unilamellar vesicles (LUVs), while their conformation was investigated in LUVs using circular dichroism (CD). The insertion of the peptide into lipid monolayers was assessed with Gibbs adsorption isotherms at a constant area, and the microenvironment around the tryptophan residue of the peptides adsorbed onto lipid vesicles was monitored by red-edge excitation shift (REES). The effect of the peptides on lipid packing was investigated by compression isotherms of lipid/peptide pre-mixed films, in which the impact of the peptide on the phase equilibrium was monitored by visualization of the Langmuir films by fluorescence microscopy. In addition, lipid bilayer phase behavior and thermotropic changes induced by these peptides were accessed by DSC. The association of all these techniques provided evidence that the N-terminus acetylation of this peptide allows deeper penetration into the membrane, disturbing the lipid-packing more efficiently and resulting in higher lytic activity.

2. Materials and methods

2.1. Chemicals and reagents

Lipids: 1-palmitoyl-2-oleoyl-*sn*-glycero-3-phosphocholine (POPC), 1-palmitoyl-2-oleoyl-*sn*-glycero-3-phosphoglycerol (POPG), 1,2-dipalmitoyl-*sn*-glycero-3-phosphocholine (DPPC) and 1,2-dipalmitoyl-*sn*-glycero-3-phosphoglycerol (DPPG) were obtained from Avanti Polar Lipids (Alabaster-Al-USA). 1-palmitoyl-2-{12-[7-nitro-2-1,3-benzoxadiazol-4-*yl*)amino]dodecanoyl}-*sn*-glycero-3-phosphocoline (NBD-PC) was from Avanti Polar Lipids (Alabaster-Al-USA). All peptides were from Genscript (Piscataway-NJ-USA) with RP-HPLC purity level > 98.5%. Chloroform and methanol, HPLC grade, were obtained from Merck (Darmstadt, Germany). Sodium chloride, sodium hydroxide, sucrose, glucose, and acrylamide were from Sigma. Ultrapure water used to prepare solutions was previously deionized in an ion exchange resin and filtered in a Millipore Milli-Q system (~18 MΩ cm).

2.2. Preparation of giant unilamellar vesicles (GUVs)

POPC and POPC:POPG (8:2 molar ratio) GUVs were prepared by the electroformation technique as described by Angelova and Dimitrov [15]. Briefly, 20 μl of a 2 mg/ml lipid chloroform/methanol solution was spread on the conductive sides of two glasses coated with indium tin oxide (ITO) and were left under vacuum for at least 3 h to remove all traces of the organic solvent. The conductive sides of two slides covered with the phospholipid film were placed facing each other and separated by a Teflon frame 2 mm thick, forming a chamber. The lipid films were hydrated by filling this chamber with 0.2 M sucrose solution. The glass slides were connected to a function generator (Minipa, MFG-4202) applying a sinusoidal tension of ~1 V amplitude and 10 Hz frequency for 2–3 h.

2.3. Observation of GUVs

Before observation, the vesicle solution was diluted with an isoosmolar glucose solution (0.2 M). Due to differences in density, the vesicles were stabilized on the bottom by gravity, and due to the differences in refractive indices between sucrose (inside) and glucose (outside), they provided an adequate contrast for the observation with phase contrast microscopy. GUVs were observed with an inverted microscope (Olympus IX-71, Tokyo, Japan) equipped with a CCD camera and an LUCPlanFLN 40x Ph2 objective. To avoid osmotic pressure effects, the osmolarities of sucrose and glucose solutions were checked with an osmometer (Osmette A 5002, Precision Systems, Inc., USA) and carefully matched. Peptide solutions prepared in glucose (0.2 M) were added to the observation chamber with a microsyringe Hamilton (Reno, NV, USA) to yield the final desired peptide concentration, 2.5, 5.0 or 10.0 μM. The quantification of GUV's shape was performed using the NIH free ImageJ software.

2.4. Preparation of multilamellar and large unilamellar vesicles (MLVs and LUVs, respectively)

MLVs of pure DPPC, pure DPPG and DPPC:DPPG (8:2 molar ratio) mixture for differential scanning calorimetry (DSC) experiments were obtained from lipids dissolved in chloroform/methanol (2:1) in round-bottom flasks, where the solvent was first dried under a stream of nitrogen, and then, stored under vacuum overnight to totally remove the organic solvent. Afterward, the lipid films were hydrated, at ~10 °C above the liquid-crystalline phase transition temperature, with HEPES buffer (HEPES 20 mM, 150 mM NaCl, pH 7.4) with or without an appropriate amount of peptide stock solution and submitted to an intense vortexing. LUVs of pure POPC and POPC:POPG (8:2 molar ratio) mixture for CD and REES experiments were prepared by extrusion of MLVs, 6 and 11 times through a polycarbonate membrane of 0.4 and 0.1 μm pore size, respectively, as described by Leite and co-authors [16]. LUVs were prepared with HEPES 5 mM, 150 mM NaF, pH 7.4 or HEPES 20 mM, 150 mM NaCl, pH 7.4 for CD and REES experiments, respectively. The size distribution was confirmed by Dynamic Light Scattering (DLS) with a Nano Zetasizer ZS90 (Malvern Instruments, Worcestershire, U.K.). The average diameter of the liposomes was 140 ± 4 nm. Only fresh vesicles were used in each experiment.

2.5. Circular dichroism (CD)

CD spectra were collected over the range 190–260 nm, using a Jasco-815 spectropolarimeter (JASCO International Co. Ltd., Tokyo, Japan) with a Peltier system to control the temperature. Spectra were obtained at 25 °C using a 0.1 cm path length cell, and averaged over 10 to 30 scans, each one at a scan speed of 50 nm/min, with at bandwidth of 1.0 nm, 0.5 s response and 0.1 nm resolution. CD spectra for 20 μM peptide concentration bound to pure POPC and POPC:POPG (8:2 molar ratio) LUVs were obtained for 0.7, 1.3 and 5.0 mM lipid concentrations. Following baseline correction, the observed ellipticity, θ (mdeg), was converted to mean residue ellipticity [Θ] (deg cm^2/dmol), using the relationship $[\Theta] = 100\theta/(lcN_r)$, where l is the path length in centimeters, c is the millimolar peptide concentration, and N_r is the number of residues in the peptide sequence. The observed mean residue ellipticity in 222 nm (Θ_{obs}) was converted to fractional helicity (f_H) by [17]:

$$f_H = \frac{(\Theta_{obs} - \Theta_C)}{\Theta_H - \Theta_C} \quad (1)$$

where Θ_C (= 1500 deg cm^2/dmol) and Θ_H are the molar ellipticity of random coil and completely helical peptide, respectively [17], and:

$$\Theta_H = (-44000 + 250T)(1 - x/N_r) \quad (2)$$

where, N_r = 18 is peptide length, x = 3 is the number of non-H-bonded CO groups in a carboxylated peptide and T = 25 °C.

2.6. Steady-state fluorescence spectroscopy

Tryptophan emission fluorescence spectra were collected with ISS PC1 spectrofluorometer (Champaign, IL, USA), using a quartz cell with 1 cm path length, thermostated at 25 °C. The emission spectra were recorded after 1 h of sample preparation. Excitation and emission slits of 2.0 nm and bandpass filter were used for all measurements. Correction for scattering was carried out by using Glan-Thomson polarizers (excitation polarized at 90° and emission at 0°) as described by Ladokhin et al. [18], and by subtracting spectra obtained at each vesicle concentration as blank. The standard deviation for the spectral shift was 1 nm.

2.7. Penetration into monolayers

Gibbs isotherms of the peptides were constructed by registering the surface pressure change of a clean NaCl 150 mM-air interface after increasing amounts of peptide were injected in the subphase. The penetration of peptides into lipid films composed of POPC, POPC:POPG (8:2 molar ratio), DPPC and DPPG were assessed in experiments at constant area using a home-made circular trough (volume 4.5 ml, surface area 7 cm^2). In these experiments, peptide solution (final concentration of 1.25 μM) was injected below the lipid-150 mM NaCl interface at an initial surface pressure (π_i) of 30 mN/m under continuous stirring. The peptide penetration into the monolayer was followed by the increase in surface pressure ($\Delta\pi$) as a function of time. All experiments were performed at 25 °C. The standard deviations were obtained from at least three measurements.

2.8. Compression isotherms

Compression isotherms of the peptides, the lipids or lipid/peptide mixtures were carried out in a Teflon trough (volume 180 mL, surface area 243 cm^2) on pure water or saline (150 mM NaCl) solution. Surface pressure (π) was measured using a Pt plate by the Wilhelmy method, and the total film area was continuously registered using a KSV Minitrough apparatus (KSV, Helsinki, Finland) enclosed in an acrylic box. Pure peptide monolayers were prepared by spreading a peptide solution in methanol onto the surface of water or saline subphase by using a microsyringe Hamilton (Reno, NV, USA). For lipid or lipid-peptide mixed monolayers, phospholipids were dissolved in chloroform/methanol (2:1 (v:v)) to a final concentration of 2.5 mM. Small drops of solutions of lipid or lipid-peptide premixed at a desired ratio were directly spread on the surface. After 10 min to allow organic solvent evaporation, the monolayers were compressed at 7 mm/min. All measurements were performed at 20°C. The determined mean molecular areas were highly reproducible, with standard deviations lower than 3% as obtained from at least three compression isotherms for each condition.

The mixing behavior of lipids and peptides can be analyzed by comparing the mean molecular area of the mixture with that of an ideal mixture calculated as [19]:

$$A_{ex} = A_{12} - (A_1X_1 + A_2X_2) \quad (3)$$

where X_1 and X_2 are the molar fractions of component 1 (lipid) and component 2 (peptide), respectively, and A_1 and A_2 are the corresponding mean molecular areas at a given surface pressure.

2.9. Fluorescence Microscopy (FM) of surface films

The lateral organization of the lipid/peptide monolayers was monitored by fluorescence microscopy during compression of the films. For these experiments, the lipid/peptide mixture was doped with 0.5 mol% of NBD-PC and spread in a Teflon trough (with a glass window) mounted on the stage of an Olympus XI inverted microscope (Olympus IX71, Tokyo, Japan) equipped with fluorescent filters and connected to a CCD camera. A mercury lamp housing was used to excite the fluorescent probe, and excitation and emission wavelengths were selected by a specific beam splitter/filter.

2.10. Differential Scanning Calorimetry (DSC)

DSC measurements were carried out using an N-DSC III (TA Instruments, USA) at a scan rate of 0.5 °C/min. Solutions were degassed for 20 min under vacuum before being loaded into the sample cell. Data analysis was done using Laugh Nano Analyze software: the buffer-buffer scan was subtracted from the raw data, and then, the curves were normalized by the lipid concentration. Several up and down scans were performed for each sample to prove the reproducibility. The calorimetric enthalpy (ΔH) was calculated by integrating the area under the peak of the heat capacity of the transition (ΔC_p) using the Eq. (4):

$$\Delta H = \int_{T_1}^{T_2} C_p dT \quad (4)$$

where T_1 and T_2 are the temperature of beginning and end of the phase transition, respectively.

3. Results and discussion

3.1. Lytic activity of L1A and ac-L1A peptides

The lytic activity of L1A and ac-L1A was investigated through the observation of GUVs by phase-contrast microscopy. Fig. 1 shows phase contrast snapshots of POPC and 8POPC:2POPG GUVs before and after peptide injection near the GUVs (5 μM final concentration). In every experiment, peptide action was followed by decreased contrast of the GUV under observation due to the reduction in concentration gradient of glucose and sucrose, as a consequence of their permeation. The time necessary to achieve complete phase-contrast loss is dependent on the peptide nature and concentration (Fig. 1A–D and Supplementary material SM-1 and SM-2), and on the vesicles compositions.

For POPC GUVs exposed to L1A, the permeation occurred after lengthy periods (300 to 1000 s depending on the peptide concentration). When 20% of POPC was changed by POPG, forming 8POPC:2POPG GUVs, the loss of contrast occurred after shorter periods (Fig. 1E), suggesting an electrostatic influence on peptide/membrane interaction. In spite of this, less charged acetylated analog induced a complete loss of the phase contrast after slightly shorter periods than L1A for both lipid compositions (Fig. 1E), which indicates an additional presence of non-electrostatic factors in the peptide/lipid interaction. Similar observations were reported for the effect of the peptide MP1 and its D2N analog [20].

The images also revealed that peptide-induced membrane permeability to sucrose and glucose occasionally induced rupture of the vesicles. In POPC GUVs, vesicle rupture occurs from 10 μM for both peptides (2% of the analyzed GUVs), while, for 8POPC:2POPG GUVs, vesicle rupture occurred at all studied peptide concentrations (5%–8% of the GUVs, depending on peptide concentration). Thus, the loss of phase contrast is most likely a result of the peptide-induced defect or pore in the membrane that, occasionally, leads to vesicle breakdown.

Interestingly, both peptides induced changes in vesicle shape only in

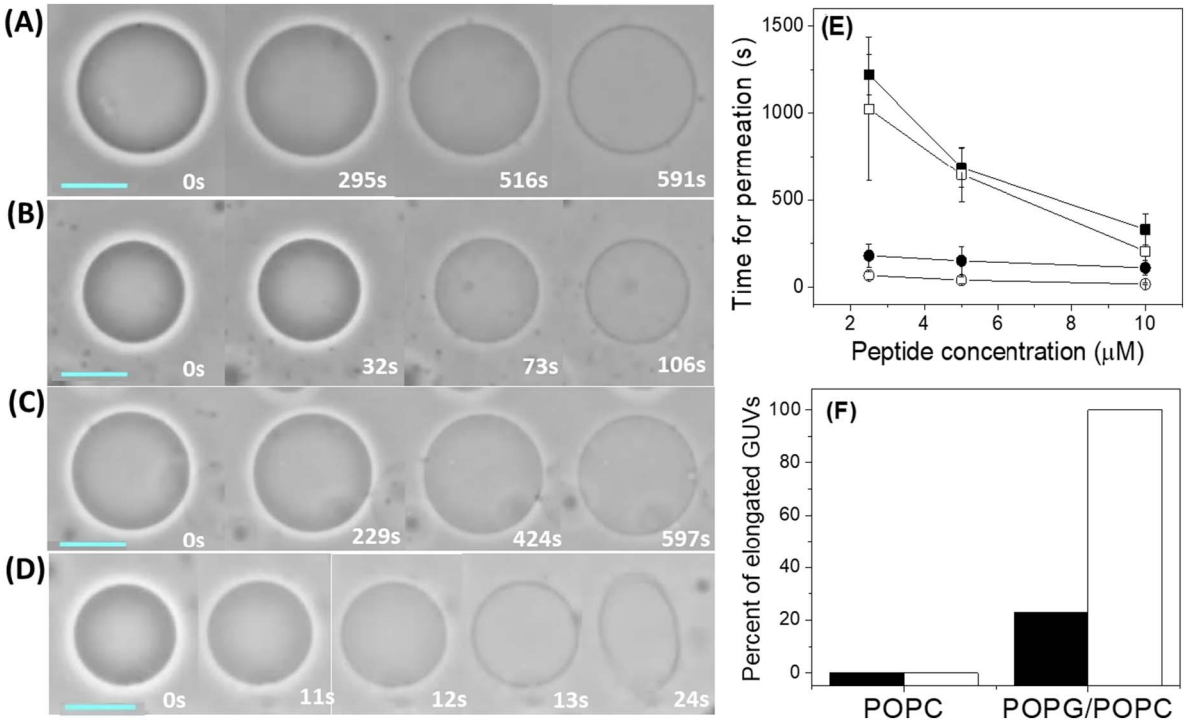

Fig. 1. The lytic activity of antimicrobial peptides investigated by experiments with GUVs. Phase contrast images of POPC (A and C) and 8POPC:2POPG (B and D) vesicles after addition of 5 μM of L1A (A-B) and ac-L1A (C-D). The first image of each sequence represents the time when the peptide was injected. The scale bars represent 20 μm. This overall trend was observed for at least 35 GUVs at each condition. (E) Average time (± standard deviation) for the GUV permeation as a function of the peptide concentration, determined in at least 35 individual GUVs. The peptides correspond to L1A (closed symbol) and ac-L1A (open symbol) in contact with vesicles composed of POPC (squares) or 8POPC:2POPG (circles). (F) Percent of GUVs with an aspect ratio higher than 1 when they are in contact with L1A (black bars) and ac-L1A (white bars) at a concentration of peptide of 5 μM.

8POPC:2POPG GUVs (Fig. 1F). In this situation, two shapes were observed, prolate and oblate (see SM-3A). The aspect ratio (AR), *i.e.*, the ratio between the longest and the shortest radius of each single GUV (see sketch shown in SM-3B), was measured for at least 35 individual vesicles. The results showed an increase of AR induced by ac-L1A for 100% of analyzed GUVs at 5 μM of peptide. On the other hand, for the same peptide concentration, this effect was less pronounced for L1A, in which ~23% of the analyzed GUVs had a non-spherical shape. This overall trend was observed for all three peptide concentrations studied.

The shape of the vesicles depends on mechanical properties of membranes [21], such as curvature, bending rigidity and membrane tension. Peptide-induced changes in vesicle shape from sphere-to-prolate/oblate therefore suggest that peptides affect these parameters [22]. This effect is not observed in POPC membranes, which may be due to the different initial mechanical properties of the anionic vesicles when compared to the zwitterionic vesicles, and also to a different effect of the peptides in each membrane composition, which may be related to the known different partition [13] and/or depth penetration of the peptides in each membrane. Regarding the mechanical properties of the POPC and the 8POPC:2POPG vesicles in the absence of peptides, fewer membrane undulations are expected in the anionic membranes [23], highlighting the changes promoted by the peptides in the 8POPC:2POPG GUVs. Shape deformations were observed for 8POPC:2POPG membranes in the presence of both peptides, but the effect was more marked in ac-L1A than in L1A, *i.e.* for the peptide that induced membrane permeability faster. Thus, a higher disruption of the membrane is induced by the acetylated peptide.

In GUV experiments, the peptide-to-lipid ratio cannot be exactly determined, and specific information, for instance about the lytic activity of peptide, is obtained for a single vesicle. Therefore, we also investigated the lytic activity of both peptides in large unilamellar vesicles (LUVs) in which the leakage of an entrapped dye is obtained from a collection of vesicles. As previously reported [24], the two methods are complementary. The leakage experiments performed with the same peptides in LUVs pointed to similar results. The leakage of anionic vesicles was found to occur at smaller peptide concentrations than the zwitterionic ones for both peptides. The peptide-to-lipid concentration ratios necessary to achieve 50% leakage (EC_{50}) after 1 min of peptide addition, were 3.5-times larger for L1A than for ac-L1A in 8POPC:2POPG vesicles (SM-4).

Despite the high lytic activity of both peptides in POPC vesicles, they lack hemolytic activity in human blood cells [12]. In addition to phosphatidylcholine lipid, mammalian cell membranes are rich in cholesterol and sphingomyelin, which may be responsible for the red cell membrane stabilization.

3.2. Conformational analysis of the peptides in lipid bilayers

The partition of the peptides into the vesicles was monitored by their change in folding once they were exposed to the vesicle interfaces, using circular dichroism (CD) experiments. The CD spectra were characterized by double minima at 222 and 208 nm for the two lipid compositions, as illustrated in Fig. 2A, at 1.3 mM of 8POPC:2POPG LUVs. The intensities of these bands increased with total lipid concentration up to 5.0 mM, when the maximum spectral change was observed. These spectra showed that the 208 nm band is more intense than the 222 nm one, suggesting that, up to this lipid-to-peptide molar concentration ratio ([L]/[P] = 250), the peptides are in monomeric form in the vesicles [25]. The helical fractions (f_H), calculated from the CD spectra (using Eq. (1)), are plotted in Fig. 2B.

In anionic 8POPC:2POPG LUVs, both peptides showed a higher helical content, which reached a maximum value at [L]/[P] = 65. The maximum helical content of the acetylated analog, with a net charge Q = + 2, was, however, almost 30% larger than that observed for L1A, with a net charge Q = + 3. At [L]/[P] = 250, L1A showed a value of 41 and 52% of the helix in zwitterionic and anionic vesicles, respectively, which means that 7 and 9 residues are in a helical conformation, while ac-L1A presented 12 residues in a helical conformation for both

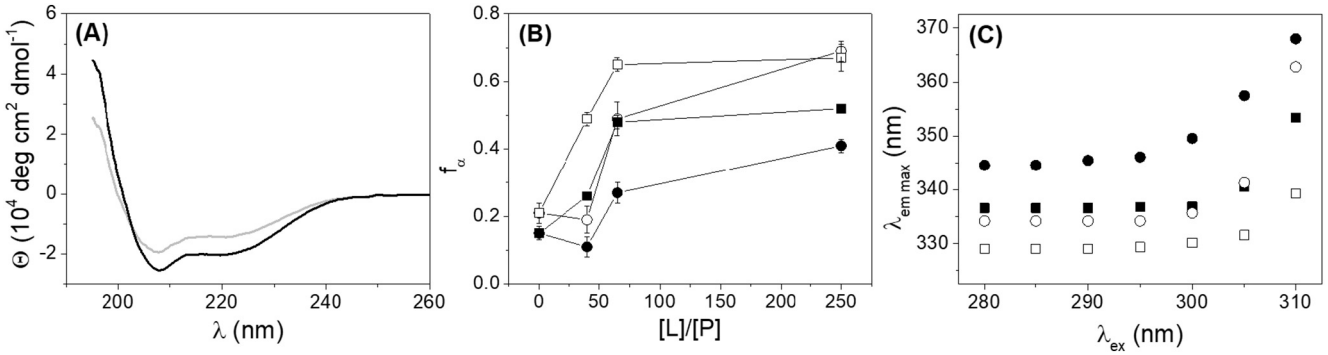

Fig. 2. (A) Circular dichroism spectra of L1A (gray line) and its acetylated analog, ac-L1A, (black line) in the presence of 1.3 mM of LUVs of 8POPC:2POPG. (B) Percent of an alpha helix in the peptides as a function of the Lipid to Peptide molar ratio for solutions with 20 μM L1A (closed symbol) and ac-L1A (open symbol) in contact with vesicles composed of POPC (circles) or 8POPC2POPG (Squares). (C) Influence of excitation wavelength (λ_{ex}) on the wavelength of maximum emission (($\lambda_{ex\ max}$) of L1A (closed symbol) and ac-L1A (open symbol) in LUVs of POPC (circle) and 8POPC:2POPG (square). Lipid to peptide ratio was 100.

vesicle compositions. L1A showed larger content in anionic than zwitterionic vesicles, indicating the importance of the electrostatic contribution in peptide folding, similar to the leakage results in GUVs and in LUVs. However, a reduction of the N-terminus charge favored the helical conformation and, at higher [L]/[P] ratio (*i.e.* 250), no difference in the helical content was observed, again indicating that non-electrostatic factors also drive ac-L1A/lipid interaction. Molecular dynamics simulations of the L1A and ac-L1A in an aqueous solution of 30% trifluoroethanol (TFE) showed that the charged N-terminus in L1A was preferentially surrounded by water molecules while the acetylated N-terminus was surrounded by TFE molecules [12]. TFE is an alcohol that induces almost the same amount of helix in the peptide as a membrane, although the mechanism of helix formation is different in both environments [17]. The *in silico* experiments indicate that the acetylated amino group prefers an environment of lower dielectric constant, a behavior similar to hydrophobic side chains. The water-solvated N-terminus prevented intra-chain CO-NH backbone H-bonds, while acetylation increased by five the NH-CO backbone H-bonds compared to the non-acetylated N-terminus [12]. These extra bonds are a consequence of the reduction of water molecules surrounding the N-terminus. In addition, the acetylated group on the N-terminus has an ability in acting as a helix cap greatly enhancing the helix stability [26]. The higher alpha-helix fraction for ac-L1A compared to L1A shown in Fig. 2 may, therefore, be related to its higher intrinsic ability for alpha-helix formation.

3.3. Changes in the environment of tryptophan upon binding to membranes

Red-edge excitation shift (REES) experiments were performed to assess the environment around tryptophan (Trp) residue. The maximum shift of Trp residue of L1A and ac-L1A in POPC and 8POPC:2POPG LUVs as a function of the excitation wavelength is shown in Fig. 2C, and the values of REES are summarized in Table 1. REES values of 13 and 4 nm were observed in POPC vesicles, for L1A and ac-L1A, respectively, while the corresponding values in the anionic vesicles were 7 and 2 nm.

REES is observed when the fluorophore relaxation time is equal to or higher than its lifetime [27]. In the interfacial region of the membrane, solvent relaxation occurs at lower rates, *i.e.*, the environment applies resistance in the reorientation of solvent dipoles, giving rise to red-edge effects [28]. Furthermore, in the interfacial polar region of the membrane, the hydrogen bond between polar head groups (except for PC headgroup) [29] and intermolecular charge interactions [30] contribute to a slowdown in solvent reorientation time. On the other hand, when the fluorophore is in an apolar environment, the maximum emission wavelength is blue-shifted with an increase in intensity. Thus, in both lipid compositions, the values of REES obtained for L1A indicate that Trp residue is localized in a restricted mobility environment, consistent with the interfacial localization of Trp residue of melittin peptide in the membrane [31].

Table 1
Tryptophan emission shift upon peptide binding and parameters from the peptide Gibbs isotherms.

Peptide	POPC		8POPC:2POPG		Gibbs isotherms		
	[a]REES (nm)	[b]SV	[a]REES (nm)	[b]SV	[c]C_{sat} (μM)	[d]Π_{sat} (mN/m)	[e]Γ_{max} (molec/Å^2)
L1A	13 ± 2	1.5	7 ± 1	3.6	0.9 ± 0.1	33 ± 3	0.035
Ac-L1A	4 ± 1	3.2	2 ± 1	6.7	0.7 ± 0.1	27 ± 1	0.020

[a] Red-edge excitation shift. The values were carried out beyond 305 nm due to artifacts of solvent Raman peak and due to low signal-to-noise ratio.
[b] The ratios between Stern-Volmer constant values in buffer and vesicle solution: extracted from [13].
[c] Minimal bulk concentration of the peptide necessary for reaching the maximal final surface pressure upon its adsorption.
[d] Final surface pressure reached by the adsorption of each peptide to a clean NaCl 150 mM-air interface at saturating bulk concentration.
[e] Higher surface excess reached by the peptides at a NaCl 150 mM-air interface,

On the other hand, the values of REES around 4–2 nm observed for the analog ac-L1A suggest that Trp residue is in a less restrictive, less polar and more flexible environment (more dynamic) [32]. Due to the preference of acetylated N-terminus for a lower dielectric constant environment than the non-acetylated one [12] the acetylated peptide penetrates into deeper regions of the membrane than L1A, which may play a role in affecting membrane curvature and general mechanical properties, thus inducing the vesicle shape deformations shown in SM-3.

The N-terminal positive charge may promote the association of the peptide with the head-group region of lipid bilayers, hampering its penetration into the hydrophobic core. These observations were reinforced by both the blue-shift emission maxima and the fluorescence quenching of Trp by acrylamide. As a consequence of a red-shifted emission, the tryptophan presents lower blue shift and is more exposed to the solute quencher. ac-L1A displays a blue-shift emission maximum 5 and 8 nm higher than L1A, in POPC and 8POPC:2POPG, respectively, suggesting that the environment around the Trp residue of ac-L1A is more hydrophobic [13]. Fluorescence quenching of the single tryptophan of these peptides by acrylamide, when the peptide was adsorbed onto an 8POPC:2POPG bilayer, showed that the acrylamide was less accessible to this residue in ac-L1A compared to L1A [13]. The smaller accessibility of the acrylamide to tryptophan indicates that the peptide, and consequently this fluorophore, is more deeply buried in the hydrophobic phase of the bilayer, thus disrupting the membrane structure to a higher extent, as observed in the GUV experiments.

3.4. Incorporation of the peptides into lipid monolayers

Lipid monolayer formed at the air-water interface is a model system that may mimic the outer or inner leaflet of the bilayer, and it has been used extensively to investigate the impact of antimicrobial peptides on lipid packing [33,34]. The first contact of the peptide with the membrane can be studied by insertion experiments of the peptide into lipid monolayers, while the effect of the incorporated peptide on the membrane structure can be assessed by compression isotherms of peptide-lipid monolayers.

In order to analyze the capability of the peptides to self-form Gibbs monolayers, we first studied the adsorption of both peptides onto a clean NaCl 150 mM-air interface. Both peptides increased the surface pressure of the clean interface, thus behaving as a surfactant. The plots of the final surface pressure *versus* peptide concentration are shown in SM-5, whilst Table 1 summarizes the main results. At bulk-saturating concentration, high surface pressures were reached for both peptides, with a value of 33 mN/m for L1A, and 27 mN/m for ac-L1A. These values are in the range (or close to it for ac-L1A) of that proposed to be comparable to lipid bilayers (30–35 mN/m, [35,36]). In this regard, it is important to remark that thermal fluctuations may lead to variations in the lateral pressure [37], and thus a sharply defined limit for this parameter cannot be assigned.

The adsorption process for L1A and for its acetylated analog reached saturation at similar bulk concentrations (slightly higher for L1A, see Table 1). From the data below these concentrations, the highest surface excess was calculated (Γ_{max}) (see Table 1 for details). If a monolayer of molecules was formed at the interface, the inverse of Γ_{max} would correspond to the mean molecular area of the adsorbed molecule. From the data in Table 1 we obtain mean molecular areas of 30 and 50 Å^2, for L1A and ac-L1A, respectively. These values are far lower than expected, since the minimal mean molecular area, which corresponds to a peptide with an alpha-helix secondary structure orientated perpendicularly to the interface, would be approximately 180 Å^2 [38]. Also, 30 and 50 Å^2 is lower than those values obtained from compression isotherms (see next section). We therefore conclude that the Gibbs monolayers formed by the peptides consist of more than one layer of accumulated molecules.

In order to investigate the effect of the presence of lipids at the interface on peptide insertion, the surface pressure of lipid monolayers was registered after injecting L1A and its acetylated analog in the subphase at a final peptide concentration of 1.25 μM (*i.e.*, larger than the saturating bulk concentration). We studied the incorporation into monolayers of pure POPC and 8POPC:2POPG mixture, both films at an initial surface pressure of 30 mN/m. Additionally, since the lipid packing in the membrane is strongly dependent on the characteristics of the lipid acyl chains, the insertion of both peptides was also monitored in DPPC and DPPG monolayers at the same initial surface pressure (30 mN/m). Saturated chains form stiffer monolayers, more ordered and closely packed, and less fluid than those containing unsaturations [39]. Representative time courses of surface pressure changes for all systems are shown in SM-6.

The change in surface pressure induced by the peptides depends on both the amount of incorporated peptide and the stiffness of the lipid monolayer. Therefore, in order to compare the effect of the peptides on monolayers of very different stiffness, we calculated the area change supported by the lipid monolayer when the peptide is inserted into the film. In order to do this, we assumed ideal mixing, and the areas at the initial and final pressures of the insertion experiments were taken from the compression isotherms of the pure lipids or mixtures of lipids. The peptide/lipid monolayers may not behave ideally but, at low peptide concentrations, this is an acceptable assumption, since we are analyzing the compression of the regions of pure lipid caused by the insertion of the peptide. Under this approximation, we considered that the area change promoted by the peptide in the lipid monolayer corresponds to the area occupied by the peptide as it penetrates into the film plus possible disruptions of the lipid film.

Table 2
Change in the surface pressure and lipid area upon peptide penetration. The data correspond to the average (± standard deviation) of three independent experiments.

	Δπ (mN/m)	[a]ΔA (Å^2)	Δπ (mN/m)	[a]ΔA (Å^2)
	L1A		ac-L1A	
POPC	1.0 ± 1.0	0.6 ± 0.5	4.0 ± 1.0	2.7 ± 0.5
8POPC:2POPG	5.0 ± 1.0	3.6 ± 0.5	8.0 ± 1.0	5.8 ± 0.5
DPPC	0.4 ± 1.0	0.0 ± 0.5	2.0 ± 1.0	0.8 ± 0.5
DPPG	3.4 ± 1.0	1.8 ± 0.5	6.0 ± 1.0	3.0 ± 0.5

[a] Area per lipid molecule occupied by the peptides.

Table 2 summarizes the results found in the insertion experiments. The incorporation of L1A into both PC monolayers was negligible. This indicates that the presence of these lipids at the interface did not favor L1A insertion into the interface compared to its insertion into clean surfaces. For DPPG films, the surface pressure increase and the area change were not negligible but the final pressure was similar to those reached by the peptide in a bare interface, indicating that the presence of the lipid film does not improve the peptide incorporation at the interface compared to a clean air-water interface. This peptide might, however, accumulate close to the polar headgroups without inducing surface pressure changes.

Conversely, ac-L1A penetrated both PC monolayers (DPPC and POPC) and PG monolayers and, like L1A, also penetrated 8POPC:2POPG monolayers. In all these experiments, the surface pressures reached larger values compared to those for peptides at clean interfaces. Comparison of the area change obtained with DPPG and with 8POPC:2POPG indicates that the changes induced by the incorporation of both peptides is ~2-times larger in the less packed monolayers (POPC:POPG), in spite of the smaller surface charge density of 8POPC:2POPG compared to DPPG. This can be explained considering that the favorable electrostatic factors derived from the charged interface are counterbalanced by steric factors, which impede the incorporation of molecules into stiff membranes such as those of DPPG.

3.5. Perturbation of the structure of lipid monolayers induced by the peptides

Next, we explored the properties of Langmuir monolayers of lipids premixed with the peptides. In these experiments, the peptides were spread together with the lipids and were therefore forced to be at the interface forming a monolayer, unlike the penetration experiments shown previously. Compression isotherms of lipid films present different compression behavior depending on the lipid packing. We took advantage of this to explore the peptide-lipid interactions in different films, using DPPC and DPPG. By choosing these lipids, we selected lipids with a phase transition from liquid-expanded (LE) to liquid-condensed (LC) at room temperature, and we were thus able to analyze the effect of the peptides in both lipid-phase states as well as during phase transition. Additionally, compression isotherms were studied in pure water and in NaCl 150 mM solutions in order to analyze the effect of the ionic strength on the peptide/lipid monolayer behavior.

In Fig. 3A, the compression isotherms of pure L1A and ac-L1A monolayers at the air-water interface indicated that both peptides formed stable films up to a surface pressure of ~19 and 20 mN/m, respectively, with molecular areas of ~140 Å^2 at close packing. When the peptides were spread on saline solutions, the isotherms shifted to higher mean molecular areas (215 Å^2) and the collapse pressure increased to 21 and 26 mN/m for L1A and ac-L1A, respectively. Similar features have been observed for other peptides such as Polybia-MP1 [38] and Bombolitin III [40]. As already stated, a peptide with an alpha-helix structure oriented perpendicularly to the interface would occupy approximately 180 Å^2 [38]. On the other hand, the theoretical

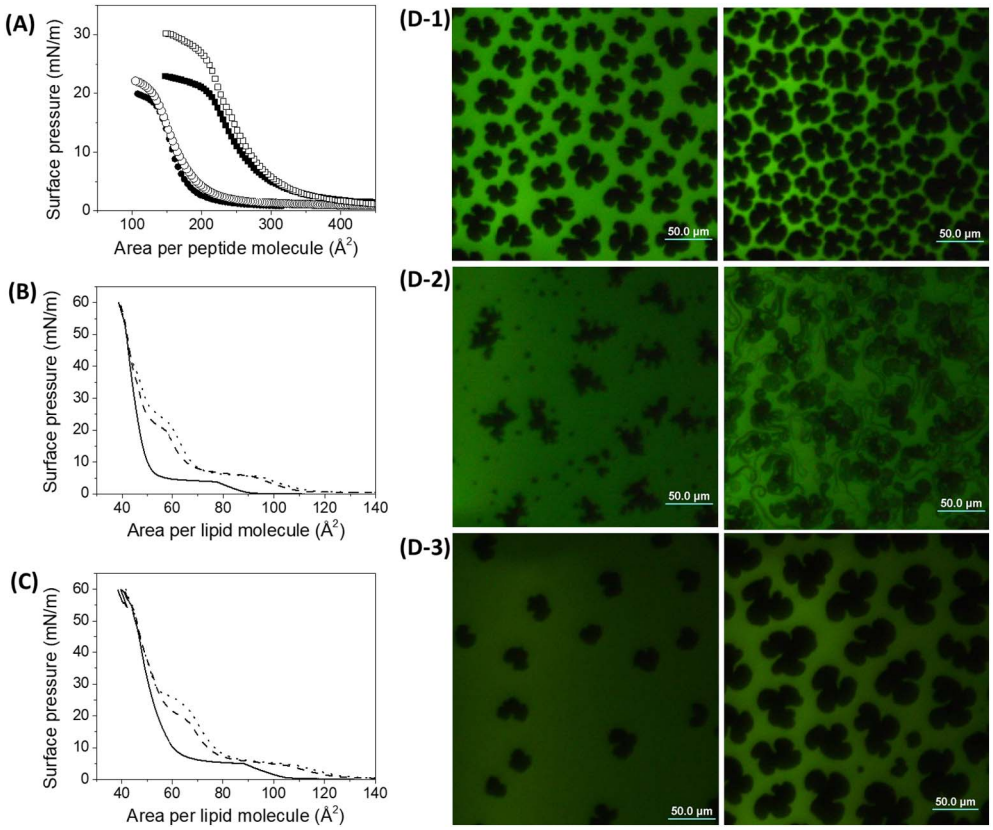

Fig. 3. Influence of peptide on the organization of DPPC monolayer. Compression isotherms of: (A) pure L1A (closed symbol) and ac-L1A (open symbol) in pure water (circle) and 150 mM NaCl, pH 7.4 (square); (B) pure DPPC (continuous line) and mixed DPPC/L1A (4.8 mol%) (dashed line) and DPPC/ac-L1A (4.8 mol%) (dotted line) monolayers on pure water and (C) saline solution. (D) Representatives FM images obtained at 5 mN/m (left) and at 7 mN/m (right) and at 20 °C. (D-1) pure DPPC in water, (D-2) DPPC/L1A for X_{L1A} = 0.048 in water and (D-3) DPPC/L1A for X_{L1A} = 0.048 in 150 mM NaCl. The monolayer contained 0.5 mol% of NBD-PC fluorescent probe. The scale bar represents 50 µm.

area occupied by an alpha-helix orientated parallel to the interface can be estimated as 22.5 Å^2 times the number of residues [38]. Thus, for a segment of 18 residues, the area would be about 400 Å^2. Therefore, the compression isotherms suggested that in both subphases, L1A and ac-L1A orient perpendicularly to the interface. In water, the peptides formed closely-packed monolayers and the slightly lower value of mean molecular area at collapse (140 Å^2 instead of 180 Å^2) may be due to pre-collapsed regions or to out-of-plane structures. In 150 mM NaCl subphases, the higher values of the mean molecular area (about 1.55 times) suggest tilting of the peptide molecules with respect to the interface.

A similar film expansion in the presence of salt was previously reported for Polybia-MP1 (with a similar extent, 1.56 times) and was explained considering that, in pure water, intermolecular salt bridges form between acidic and basic residues, which are more prone to occur at low ionic strength [38]. The similarity between L1A, ac-L1A, and MP1 is the concomitant presence of acidic and basic residues as third or fourth neighbors. We therefore propose that in both L1A and ac-L1A films, counter-ions of the subphase interact with these acidic and basic residues, competing with the intermolecular salt bridges. Therefore, at high ionic strength the peptide-peptide attractive interaction is disfavored, and a structure where the acidic and basic residues interact with the aqueous solution is favored. This emphasizes the importance of lateral electrostatic interaction between the ionizable groups forming salt bridges to define the structure of the peptides at the air-water interface. As was observed previously for Polybia-MP1 peptide [38], the collapse pressure of the film was lower when the peptides were oriented more perpendicularly to the interface than when they were tilted, *i.e.* the peptide remained at the interface up to lower surface tensions, suggesting a higher stability of the monolayer with the peptides in the latter configuration.

In DPPC monolayers, the LE to LC phase transition is observed at approximately 4 mN/m at 20 °C in both pure water and 150 mM NaCl solution (continuous line in Fig. 3B and C, respectively). Fig. 3B shows π *vs* A isotherms of films of pure DPPC and DPPC co-spread with 4.8 mol% of L1A or ac-L1A onto the air-water interface (note that the x-axis corresponds to the area per lipid molecule, without considering the peptide). In the presence of L1A or ac-L1A, the mean molecular area was slightly larger than the ideal one (see Table 3), especially for ac-L1A. This result, together with the increase in the LE/LC transition pressure of DPPC (about 2 mN/m), indicates mixing of the peptides with lipids preferentially in the LE state. A second change induced by the peptides was the presence of a quasi-plateau at ~19 and 21 mN/m for L1A and ac-L1A, respectively. These regions correspond to the pressure at which the peptides were squeezed out from the interface. Similar behavior was observed for the peptides Polybia-MP1 [38], hNPY and Y20P-NPY [41] and Bombolitin III [40]. The FM images obtained for DPPC/L1A and DPPC/ac-L1A monolayers (4.8 mol% of peptide) showed that both peptides co-crystallize with the zwitterionic lipid, inducing changes in the morphology of the solid domains from triskelion to a branched shape (see Fig. 3D-2 for L1A and Supplementary material SM-7B for ac-L1A). Similar results were also obtained for

Table 3
Collapse pressure of the peptides and excess mean molecular area of the mixtures at 15 mN/m.

	[a](mN/m) and (Å^2)[**]					
	Only peptide		Mixed with DPPC		Mixed with DPPG	
Peptides	Water	Salt	Water	Salt	Water	salt
L1A	19[a]	21[a]	19[a] (+5)[b]	20[a] (+1)[b]	21[a] (+8)[b]	29[a] (−1.3)[b]
Ac-L1A	20[a]	26[a]	21[a] (+8)[b]	25[a] (+2)[b]	27[a] (+11)[b]	31[a] (+6)[b]

[a] Collapse pressure of L1A and ac-L1A1 films obtained from compression isotherms showed in the Fig. 3A and peptide/lipid mixed films in the Figs. 3B, C, 4A, and 5A. The standard error of 1 mN/m.

[b] Excess mean molecular area calculated from compression isotherms at 15 mN/m showed in the Figs. 3, 4 and 5 using the Eq. (4). Standard error of 3.

DPPC/MP1 monolayers [38], and this was correlated with the presence of acidic and basic residues forming salt bridges that allow the peptides to form compact films and coexist with the lipid in the LC phase. Given the similitude of the peptides, we propose a similar explanation for the results shown here.

On the other hand, in the 150 mM NaCl subphase, the excess mean molecular area was negligible (see Table 2), and the quasi-plateau in which the peptide molecules were squeezed out to the subphase was similar to that in films of pure peptide (Fig. 3C). Furthermore, in this condition, no changes in the phase transition pressure and domain morphology were detected (see Fig. 3D-2 for L1A and Supplementary material SM-7C for ac-L1A). All these observations suggest that, in the 150 mM NaCl subphase, the peptides did not mix with the lipids and coexisted in the probe-enriched regions with DPPC in the LE state, thus increasing the area occupied by the probe (compare SM-7A for pure lipid with Figs. 3D-3 and SM-7C for L1A/DPPC and ac-L1A/DPPC, respectively).

Mixed films of DPPG with L1A and ac-L1A (4.8 mol%) on pure water showed a higher excess mean molecular area than in the mixtures with DPPC (Table 3). Furthermore, the pressure at which the peptide molecules were squeezed out from the interface increased by 2 mN/m (for L1A) and 7 mN/m (for ac-L1A) compared to the collapse pressure of the pure peptide (see Fig. 4A).

Since pure DPPG monolayers on water were in the LC state from lift-off up to collapse (continuous line in Fig. 4A), the fluorescent probe did not completely mix with the lipid and the FM images revealed fluorescent regions with irregular shapes, which corresponded to regions with accumulated probe, almost segregated from the lipid (Fig. 4B).

In mixed films of DPPG/L1A (4.8 mol%), the FM images showed an increase in the area occupied by the fluorescent probe from about 20% to 44% (Fig. 4C). This difference is larger than that expected for an increment caused only by the presence of the peptide in these regions (~10%), indicating that the peptide, located in the probe-enriched regions, is dragging DPPG molecules to this more expanded phase, increasing the amount of lipids in a disorder state. This correlates with the positive excess area determined from the isotherm (Table 3) and was more pronounced for acetylated peptide, as shown in Fig. 4D, in agreement with the higher value for the excess area. The fluorescently labeled regions were, for this peptide, three times larger than those in the absence of the peptide. Such an increment reveals that ac-L1A drags DPPG molecules to the LE phase state more efficiently than L1A, thus generating a more favorable environment around the peptide and remaining at the interface up to larger surface pressures.

At the highest tested surface pressures (images at the right), the three systems appeared similar, which correlates with the similarity in the compression isotherms at high pressures, and indicates that, at these pressures, only the lipid remained at the interface.

DPPG molecules have an ionizable head group with a pKa of 2.9 [42], and therefore DPPG monolayers are expected to be fully ionized at the pH (7.4) utilized and high ionic strength. In contrast, in pure water, the surface pH is expected to be lower than the bulk pH, and consequently the DPPG monolayer is not expected to be fully ionized [43]. The change in the ionization state of the PG groups led to more expanded films on 150 mM NaCl, and in this condition the DPPG-pure monolayers display an LE-LC phase transition. The surface pressure for the phase transition therefore depends on the subphase composition. In pure water, DPPG films were in the LC state from lift-off, whilst in 150 mM NaCl, LE-LC phase coexistence occurs at 6 mN/m (continuous line in Fig. 5A). It is important to emphasize that a decrease in surface pH is expected in the case of a surface with evenly distributed charges is considered. When a PG molecule is located near the peptide, the situation is much more complex, and simply considering a Gouy-Chapman distribution of ions as in ref. [43] may not be valid. Furthermore, the ionization state of the peptide is very probably sensitive

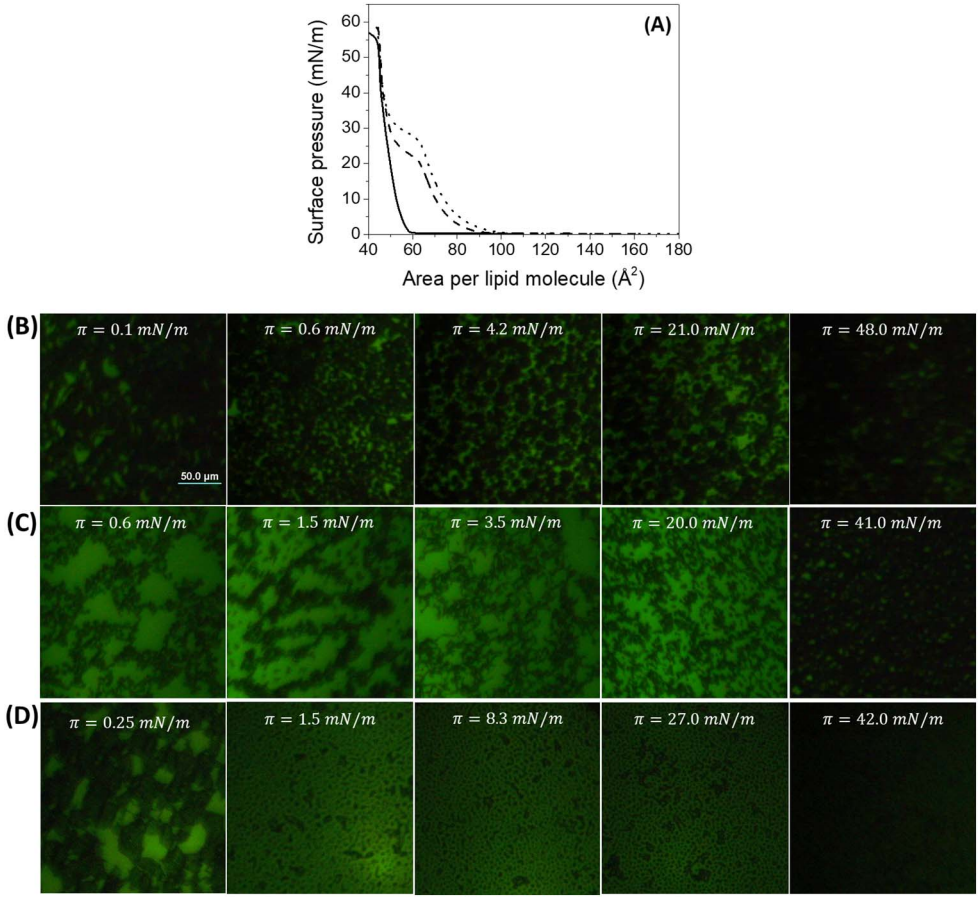

Fig. 4. Compression isotherms of pure DPPG (continuous line) and mixed DPPG/L1A (4.8 mol%) (dashed line) and DPPG/ac-L1A (4.8 mol%) (dotted line) monolayers on pure water (A). Influence of peptide on the organization of DPPG monolayer in water. Representatives FM images of monolayers composed of pure DPPG (B) and DPPG/L1A (C) and DPPG/ac-L1A (D) for a $X_{peptide}$ = 0.048 spread on pure water and registered at 20 °C and indicated surface pressures. The monolayer contained 0.5 mol% of NBD-PC fluorescent probe. The scale bar represents 50 µm.

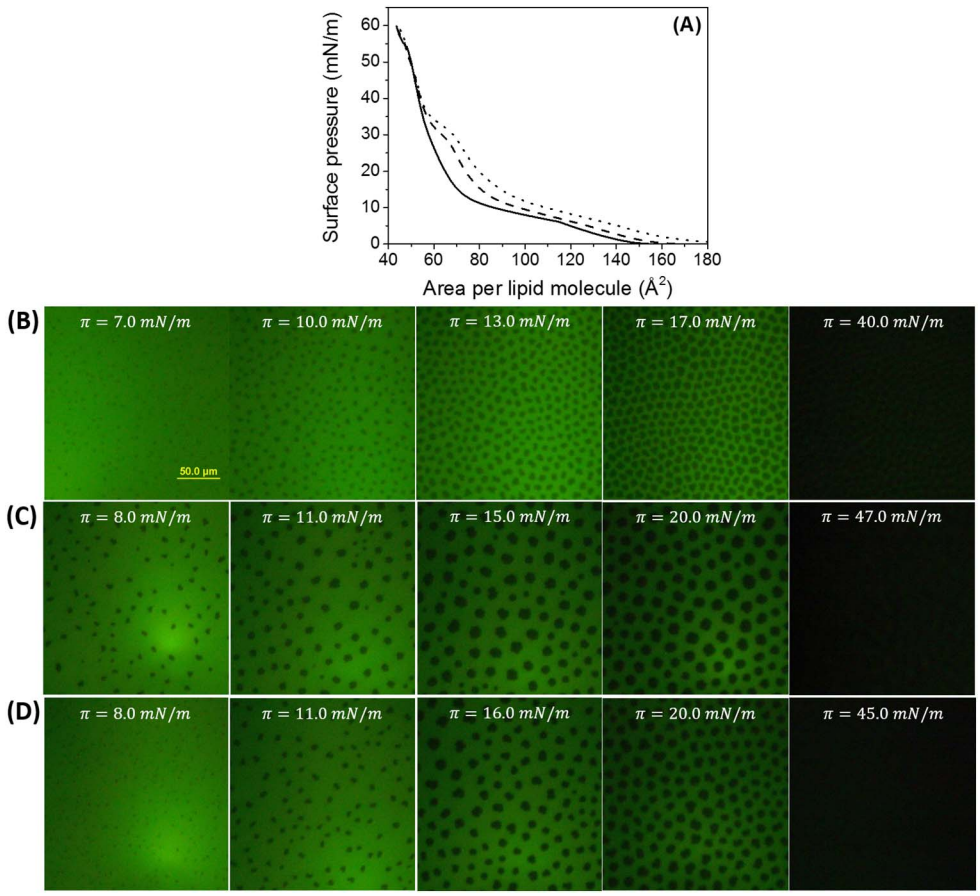

Fig. 5. Compression isotherms of pure DPPG (continuous line) and mixed DPPG/L1A (4.8 mol%) (dashed line) and DPPG/ac-L1A (4.8 mol%) (dotted line) monolayers on saline solutions (A). Influence of peptide on the organization of DPPG monolayer in saline solution. Representatives FM images of monolayers composed of pure DPPG (B) and DPPG/L1A (C) and DPPG/ac-L1A (D) for a $X_{peptide}$ = 0.048 spread on the saline solution and registered at 20 °C and indicated surface pressures. The monolayer contained 0.5 mol% of NBD-PC fluorescent probe. The scale bar represents 50 µm.

to the environment, being thus different at the interface than in bulk, giving further complexity to this issue.

In 150 mM NaCl subphases, the compression isotherms of mixed films of DPPG/peptides (4.8 mol% of L1A or of ac-L1A) showed positive excess areas only for ac-L1A (see Table 3). Regarding the film collapse, the peptide was squeezed out of the interface at pressure values higher than the collapse pressure of each pure peptide, indicating lipid-peptide mixing and a stabilization of the peptides at the interface.

FM images of pure DPPG monolayers in saline solution are in complete agreement with the compression isotherms, revealing small and roughly circular domains in LE-LC phase coexistence (Fig. 5B). On further compression, domain growth was observed, until they fuse at high surface pressure when the phase transition was completed.

In mixed films of DPPG/L1A, domain nucleation was observed at a slightly higher surface pressure (~8 mN/m) (Fig. 5C). This can also be observed in the isotherm (Fig. 5A), but not so clearly since the transition is blurred. Further compression leads to the growth of domains with a slightly larger size than in the pure lipid. The percentage of areas occupied by the fluorescently labeled phase was similar both in the absence and in the presence of the peptide, thus indicating that the peptide is located in both regions or that some peptide molecules were excluded from the interface and remained associated to the lipid headgroups.

In the presence of ac-L1A, the formation of the solid domains was observed at a higher surface pressure than those in pure lipid film. In the isotherm of this mixture, a phase transition corresponding to the appearance of the domains cannot be detected. The behavior of films both with and without peptide was similar when comparing different surface pressures (higher in DPPG/ac-L1A than in pure DPPG films, see Fig. 5B and D, respectively). This can be explained considering that the peptide mixes preferably with the DPPG lipid in the expanded phase, and thus lipids remained in this phase state up to higher surface pressures.

At surface pressures higher than 36 mN/m, the peptide was absent at the interface and the bright film region could not be observed, as occurred in the other systems, *i.e.*, only the lipid remained at the interface.

The configurations explored during the experiments compressing the pure peptides are probably not populated during the peptide-membrane interaction, since a pure peptide film is not expected to form during the incorporation of peptide into membranes. Furthermore, as stated above, in the premixed compression isotherm the peptides are forced to be at the interface, and the whole range of possible mean molecular areas is explored. However, these experiments advanced our understanding of peptide-lipid behavior; for instance, from the compression experiments performed in pure water and in 150 mM NaCl, we were able to detect the formation of salt-bridges between the acidic and basic residues of both peptides, which may also form and play a role between the peptides inside the membrane.

When these intermolecular interactions between peptides occurred, closely-packed films were able to form, and the peptides coexisted with the lipids in the condensed state. In saline solutions, the salt-bridges were disfavored and the peptides were localized in the probe-enriched regions, *i.e.*, the more expanded regions of the monolayers. In DPPC mixed films, peptides and lipids did not mix under these conditions. On the contrary, in DPPG/peptide films the peptide and the lipid showed mixing behavior in both saline and pure water subphases. The mixture of ac-L1A and DPPG was almost unaffected by the addition of NaCl, meaning that the DPPG-peptide properties were independent of the presence of ions in the subphase. In the case of L1A, the positive charge in the N-terminal probably favored its association with the head-group region of the lipids, and peptide/lipid interactions were influenced by the addition of salt.

The presence of salt in the subphase modified not only pure peptide

behavior but also pure DPPG behavior. At high ionic strength, peptide-peptide electrostatic interactions decrease, as described above, but, at the same time, peptide-lipid interactions may increase due to an increase in the degree of ionization of the lipids, leading to a very complex panorama which cannot be completely explained at this stage.

It is important to remark that both peptides disrupted the anionic lipid monolayer to a greater extent than the zwitterionic one. In addition, the effect promoted by the acetylated analog was more marked, indicating that the peptide/lipid interaction is not only driven by electrostatics. Positive deviations from ideality were found, suggesting an increased lipid disorder when the peptide was incorporated into the monolayer. We propose that the peptides generate a more favorable environment inside the condensed monolayers, disordering the hydrocarbon chains of the nearby lipid molecules and preventing them from forming stiff films.

3.6. The effects of L1A and the acetylated analog on the thermotropic properties of the lipid bilayer

Differential scanning calorimetry (DSC) experiments were performed to investigate the impact of peptide penetration on the thermotropic properties of zwitterionic and anionic lipids, DPPC and DPPG, respectively, and of 8DPPC:2DPPG mixture. Fig. 6 shows the DSC curves of the second heating scan in the absence and in the presence of L1A and ac-L1A. The thermodynamic parameters are summarized in Table 4.

The effect of L1A on the zwitterionic DPPC vesicles was modest, as the thermogram is similar to those of pure DPPC, consistent with a weak L1A/DPPC interaction. Surprisingly, a splitting in the phase transition peak was observed for the acetylated analog (see zoom in Fig. 6A), probably due to the formation of peptide-enriched (attributed to the low broad transition at 40.6 °C corresponding to the higher perturbed lipid region) and peptide-poor (which resemble the pure lipid transition at 41.3 °C and corresponding to unperturbed lipid molecules) regions. In this condition, the pre-transition (which correspond to the transition from the lamellar gel phase ($L_{\beta'}$) to the rippled gel phase ($P_{\beta'}$) [44]) was abolished. The disappearance of this less energetic pre-transition, which is very sensitive to the presence of impurities, and the split in the main phase transition peak, indicate that the acetylated peptide produces a modest destabilization of the condensed phase of DPPC MLVs.

In the case of DPPG, the presence of both peptides abolished the pre-transition peak and the main transition peak was slightly shifted to a higher temperature. L1A led to a slight decrease in the enthalpy of the main transition (ΔH_m), while its acetylated analog produced a strong decrease in ΔH_m (Table 4). The interaction between cationic peptides and anionic lipid surface was shown to induce a screening of the lipid charge and, consequently, the charge-charge repulsion of the PG head-groups decreased, with a concomitant increase of the T_m value due to stabilization of the gel phase [45,46]. In addition, change in the enthalpy of the main transition can be related to the localization of the peptide in the lipid bilayer. In this regard, as proposed by Papahadjopoulos and co-authors, [47] if an increase in the T_m is accompanied by an increase of the ΔH_m, the peptide/lipid interaction is expected to occur on the vesicle surface. In contrast, if both T_m and ΔH_m strongly decrease, beside from the electrostatic contribution, the interaction has a non-electrostatic component and the peptide is inserted into the hydrophobic core of the bilayer. The ΔT_m observed here for the two peptides (~1.0 °C) is very close to experimental error (± 0.5 °C), while the reduction in ΔH_m seems to be more reliable, indicating that the peptides perturb the lipid packing. This is in concordance with the compression isotherms, where a stabilization of the LE (disordered) phase was detected and with the proposition that the peptide drags lipids to this phase.

Regarding L1A/DPPG interaction, the slight reduction of enthalpy suggests that the peptide strongly interacts with the lipid head-groups with a slight penetration into the hydrophobic core. This was also observed in monolayer experiments in similar salt conditions, in which L1A molecules were unable to penetrate the DPPG monolayer at 30 mN/m (Table 2).

For the analog, ac-L1A, the enthalpy was reduced by ~50%, suggesting disruption of the intra and intermolecular van der Waals interactions, which indicates that the peptide penetrates deeply into the hydrophobic core perturbing the lipid-packing, [46,48] suggesting the importance of non-electrostatic contributions in the ac-L1A/DPPG interaction. This effect was also observed in monolayer experiments (Table 2), in which the acetylated analog induced higher change in the surface pressure of DPPG films and more pronounced monolayer expansion (at the same ionic strength). Furthermore, this result is also consistent with a deeper penetration of peptide into the lipid bilayer observed from the lower red-edge shift (see Table 1), and with the strong effect on the mechanical properties of GUVs. It was observed previously with molecular dynamics simulations of these peptides in aqueous TFE 30% solution that the acetylation of the N-terminus provided higher contact of the terminal region with TFE which is less polar than water. Thus, the effect of acetylation is more likely to be due to this preference of the N-terminus for a less polar environment. As a consequence of this deeper penetration of the acetylated analog, the stress induced in the bilayer leads to higher lytic efficiency.

In the 8DPPC/2DPPG mixture, both peptides induced a similar behavior to that observed in DPPG vesicles. L1A interacts mainly with the head group region on the membrane, while its acetylated analog penetrates deeper into the hydrophobic chain on the anionic bilayer. Interestingly, with only 20% of anionic lipid, ac-L1A induced a reduction of 35% of the enthalpy.

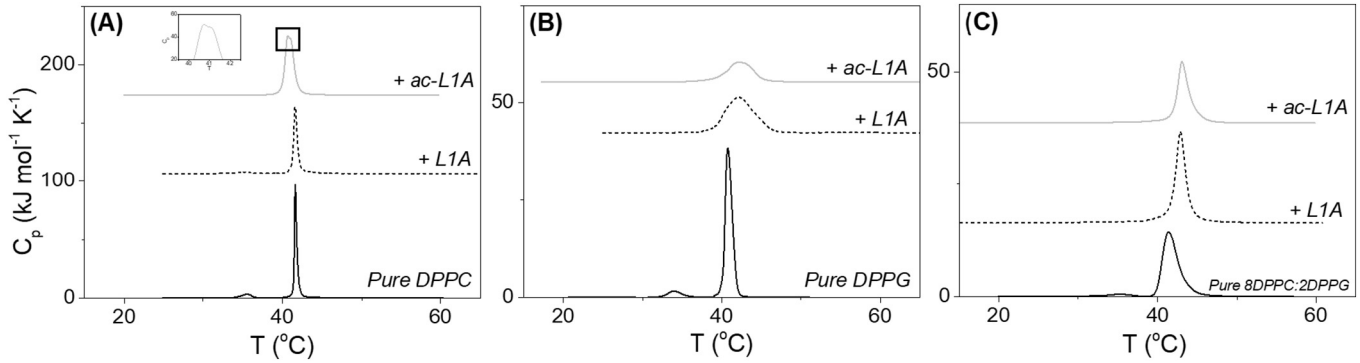

Fig. 6. Impact of peptide on the thermotropic phase behavior of zwitterionic and anionic MLVs: DSC heating thermograms of DPPC (A), DPPG (B) and 8DPPC:2DPPG (C) mixture in the absence (black lines) and in the presence of L1A (dash-dot lines) and ac-L1A (gray lines) acquired at 0.5 °C/min. For DPPC, a zoom of the peak in the presence of ac-L1A is depicted as an inset. The lipid-to-peptide ratio was 30:1 for all systems.

Table 4
Thermodynamic parameters of DPPC, DPPG and DPPC/DPPG MLVs in the presence of L1A and ac-L1A peptides obtained by DSC.

	DPPC			DPPG			8DPPC/2DPPG		
	pure	+ L1A	+ ac-L1A	pure	+ L1A	+ ac-L1A	pure	+ L1A	+ ac-L1A
[a]T_m (°C)	41.6 ± 0.5	41.6 ± 0.5	41.3 ± 0.5	41.3 ± 0.5	42.3 ± 0.5	42.3 ± 0.5	41.4 ± 0.5	43.0 ± 0.5	43.0 ± 0.5
[a]ΔH_m (kJ/mol)	41.0	38.6	46.0	42.0	40.5	23.0	38.0	37.0	25.0

[a] The values of T_m and ΔH_m are in agreement with literature [45,49–51].

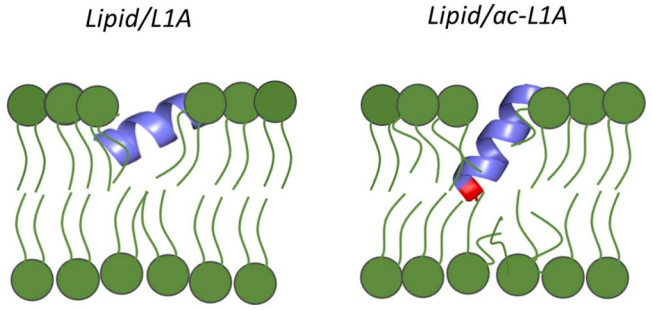

Fig. 7. Positioning of peptides into the bilayer: right: ac-L1A, and left: L1A.

4. Conclusions

The positive charge of the antimicrobial peptide is believed to be a key feature in its association with the target membranes. In line with this, L1A and ac-L1A both showed a stronger affinity for anionic than for zwitterionic vesicles. However, the present findings indicate that a lower positive net charge in the peptide may not necessarily translate to a less favorable membrane-peptide association.

The peptide-lipid interaction and consequent membrane perturbation were studied with a variety of techniques and several model membranes, and all the results agree that the effect promoted in a membrane by L1A and its analog was higher for anionic membranes and for the acetylated peptide. The evidence gathered here strongly suggests that the peptide disturbs the membrane by inserting its N-terminus into the lipid core of the bilayer. The acetylated peptide is able to penetrate into deeper regions of the membrane; a scheme of this is plotted in Fig. 7. In this way, the acetylated analog probably induces a higher perturbation in the bilayer, leading to more efficient leakage.

The findings presented here may be helpful in understanding how the N-terminal charge disfavors the deeper penetration of peptides into vesicles, and highlight the importance of the concomitant presence of acidic and basic residues in the peptide sequence as third or fourth neighbors that stabilize the peptide in the hydrophobic core. Despite the charge reduction at the N-terminus, acetylation has an important effect on the peptide secondary structure, its insertion into the bilayer and on lipid-packing perturbation.

Transparency document

The Transparency document associated with this article can be found, in the online version.

Acknowledgments

The authors acknowledge financial support from São Paulo Research Foundation - FAPESP (J.R.N. grants #2015/25619-9, and D.S.A has a Post-doctorate fellowship, grants #2015/25620-7). D.S.A. is also grateful to PROPe-UNESP for the fellowship that enabled the present study to be commenced. We would also like to thank UNESP and CAPES for their support in this research project. J.R.N. is a researcher for Brazil's National Council for Scientific and Technological Development (CNPq). N.W. is a researcher of CONICET-Argentina.

Appendix A. Supplementary data

Supplementary data to this article can be found online at https://doi.org/10.1016/j.bbamem.2017.12.018.

References

[1] M. Zasloff, Antimicrobial peptides of multicellular organisms, Nature 415 (2002) 389–395.
[2] K.A. Brogden, Antimicrobial peptides: pore formers or metabolic inhibitors in bacteria? Nat. Rev. Microbiol. 3 (2005) 238–250.
[3] L.T. Nguyen, E.F. Haney, H.J. Vogel, The expanding scope of antimicrobial peptide structures and their modes of action, Trends Biotechnol. 29 (2011) 464–472.
[4] G. Wang, Human antimicrobial peptides and proteins, Pharmaceuticals (Basel) 7 (2014) 545–594.
[5] M.R. Yeaman, N.Y. Yount, Mechanisms of antimicrobial peptide action and resistance, Pharmacol. Rev. 55 (2003) 27–55.
[6] M. Dathe, T. Wieprecht, Structural features of helical antimicrobial peptides: their potential to modulate activity on model membranes and biological cells, Biochim. Biophys. Acta Biomembr. 1462 (1999) 71–87.
[7] A.S. Ladokhin, S.H. White, Protein chemistry at membrane interfaces: non-additivity of electrostatic and hydrophobic interactions, J. Mol. Biol. 309 (2001) 543–552.
[8] S. Finger, A. Kerth, M. Dathe, A. Blume, The efficacy of trivalent cyclic hexapeptides to induce lipid clustering in PG/PE membranes correlates with their antimicrobial activity, Biochim. Biophys. Acta Biomembr. 1848 (2015) 2998–3006.
[9] H. Zhan, T. Lazaridis, Influence of the membrane dipole potential on peptide binding to lipid bilayers, Biophys. Chem. 161 (2011) 1–7.
[10] G. Beschiaschvili, J. Seelig, Peptide binding to lipid membranes. Spectroscopic studies on the insertion of a cyclic somatostatin analog into phospholipid bilayers, BBA-Biomembranes 1061 (1991) 78–84.
[11] C.M. Shepherd, K.A. Schaus, H.J. Vogel, A.H. Juffer, Molecular dynamics study of peptide-bilayer adsorption, Biophys. J. 80 (2001) 579–596.
[12] L.P.M. Zanin, A.S. de Araujo, M.A. Juliano, T. Casella, M.C.L. Nogueira, J. Ruggiero Neto, Effects of N-terminus modifications on the conformation and permeation activities of the synthetic peptide L1A, Amino Acids 48 (2016) 1433–1444.
[13] L.M.P. Zanin, D.S. Alvares, M.A. Juliano, W.M. Pazin, A.S. Ito, J. Ruggiero Neto, Interaction of a synthetic antimicrobial peptide with model membrane by fluorescence spectroscopy, Eur. Biophys. J. 42 (2013) 819–831.
[14] R.M. Epand, R.F. Epand, Lipid domains in bacterial membranes and the action of antimicrobial agents, Biochim. Biophys. Acta Biomembr. 1788 (2009) 289–294.
[15] M.I. Angelova, D.S. Dimitrov, Liposome electroformation, Faraday Discuss. Chem. Soc. 81 (1986) 303–311.
[16] N.B. Leite, L.C. Da Costa, D.S. Alvares, M.P. Dos Santos Cabrera, B.M. De Souza, M.S. Palma, J. Ruggiero Neto, The effect of acidic residues and amphipathicity on the lytic activities of mastoparan peptides studied by fluorescence and CD spectroscopy, Amino Acids 40 (2011) 91–100.
[17] P. Luo, R.L. Baldwin, Mechanism of helix induction by trifluoroethanol: a framework for extrapolating the helix-forming properties of peptides from trifluoroethanol/water mixtures back to water, Biochemistry 36 (1997) 8413–8421.
[18] A.S. Ladokhin, S. Jayasinghe, S.H. White, How to measure and analyze tryptophan fluorescence in membranes properly, and why bother? Anal. Biochem. 285 (2000) 235–245.
[19] S. Ali, J.M. Smaby, H.L. Brockman, R.E. Brown, Cholesterol's interfacial interactions with galactosylceramides, Biochemistry 33 (1994) 2900–2906.
[20] M.P. Dos Santos Cabrera, D.S. Alvares, N.B. Leite, B. Monson De Souza, M.S. Palma, K.A. Riske, J. Ruggiero Neto, New insight into the mechanism of action of wasp mastoparan peptides: lytic activity and clustering observed with giant vesicles, Langmuir 27 (2011) 10805–10813.
[21] D.D. Lasic, Y. Barenholz, Handbook of Nonmedical Applications of Liposomes: Theory and Basic Sciences, CRC Press, 1996.
[22] H.G. Dobereiner, Properties of giant vesicles, Curr. Opin. Colloid Interface Sci. 5 (2000) 256–263.
[23] O. Mertins, R. Dimova, Insights on the interactions of chitosan with phospholipid vesicles. Part I: effect of polymer deprotonation, Langmuir 29 (2013) 14545–14551.
[24] D.S. Alvares, T.G. Viegas, J. Ruggiero Neto, Lipid-packing perturbation of model membranes by pH-responsive antimicrobial peptides, Biophys. Rev. 9 (2017) 669–682.
[25] K. Matsuzaki, O. Murase, H. Tokuda, S. Funakoshi, N. Fujii, K. Miyajima, Orientational and aggregational states of magainin 2 in phospholipid bilayers,

Biochemistry 33 (1994) 3342–3349.
[26] A. Chakrabartty, A.J. Doig, R.L. Baldwin, Helix capping propensities in peptides parallel those in proteins, Proc. Natl. Acad. Sci. U. S. A. 90 (1993) 11332–11336.
[27] A. Chattopadhyay, Exploring membrane organization and dynamics by the wavelength-selective fluorescence approach, Chem. Phys. Lipids 122 (2003) 3–17.
[28] S.S. Rawat, D.A. Kelkar, A. Chattopadhyay, Monitoring gramicidin conformations in membranes: a fluorescence approach, Biophys. J. 87 (2004) 831–843.
[29] J.M. Boggs, Lipid intermolecular hydrogen bonding: influence on structural organization and membrane function, Biochim. Biophys. Acta Rev. Biomembr. 906 (1987) 353–404.
[30] P.L. Yeagle, The Membranes of Cells, Elsevier Science, 1987.
[31] A. Chattopadhyay, S.S. Rawat, D.V. Greathouse, D. a Kelkar, R.E. Koeppe, Role of tryptophan residues in gramicidin channel organization and function, Biophys. J. 95 (2008) 166–175.
[32] J. Seelig, Deuterium magnetic resonance: theory and application to lipid membranes, Q. Rev. Biophys. 10 (1977) 353.
[33] L.A. Worthman, K. Nag, P.J. Davis, K.M. Keough, Cholesterol in condensed and fluid phosphatidylcholine monolayers studied by epifluorescence microscopy, Biophys. J. 72 (1997) 2569–2580.
[34] A. Fischer, M. Lösche, H. Möhwald, E. Sackmann, On the nature of the lipid monolayer phase transition, J. Phys. Lett. 45 (1984) 785–791.
[35] D. Marsh, Lateral pressure in membranes, Biochim. Biophys. Acta Rev. Biomembr. 1286 (1996) 183–223.
[36] R.A. Demel, W.S.M. Geurts van Kessel, R.F.A. Zwaal, B. Roelofsen, L.L.M. van Deenen, Relation between various phospholipase actions on human red cell membranes and the interfacial phospholipid pressure in monolayers, BBA-Biomembranes 406 (1975) 97–107.
[37] M.C. Phillips, D.E. Graham, H. Hauser, Lateral compressibility and penetration into phospholipid monolayers and bilayers membranes, Nature 254 (1975) 154–156.
[38] D.S. Alvares, M.L. Fanani, J. Ruggiero Neto, N. Wilke, The interfacial properties of the peptide Polybia-MP1 and its interaction with DPPC are modulated by lateral electrostatic attractions, Biochim. Biophys. Acta Biomembr. 1858 (2016) 393–402.
[39] G.L. Gaines, Insoluble Monolayers at Liquid-gas Interfaces, Interscience Publishers, New York, 1966.
[40] G. Signor, S. Mammi, E. Peggion, H. Ringsdorf, A. Wagenknecht, Interaction of bombolitin III with phospholipid monolayers and liposomes and effect on the activity of phospholipase A2, Biochemistry 33 (1994) 6659–6670.
[41] M. Dyck, A. Kerth, A. Blume, M. Lo, Interaction of the neurotransmitter, neuropeptide Y, with phospholipid membranes: infrared spectroscopic characterization at the air/water, Interface (2006) 22152–22159.
[42] G. Cevc, D. Marsh, Phospholipid Bilayers: Physical Principles and Models, Wiley, New York, 1987.
[43] N. Wilke, Lipid monolayers at the air–water interface: a tool for understanding electrostatic interactions and rheology in biomembranes, Adv. Planar Lipid Bilayers Liposomes, 1st ed, Elsevier Inc, 2014, pp. 51–81.
[44] R.N. McElhaney, Differential scanning calorimetric studies of lipid-protein interactions in model membrane systems, Biochim. Biophys. Acta 864 (1986) 361–421.
[45] A. Arouri, M. Dathe, A. Blume, Peptide induced demixing in PG/PE lipid mixtures: a mechanism for the specificity of antimicrobial peptides towards bacterial membranes? Biochim. Biophys. Acta Biomembr. 1788 (2009) 650–659.
[46] F.A. Chains, R.N.A.H. Lewis, N. Mak, R.N. Mcelhaney, A Differential Scanning Calorimetric Study of the Thermotropic Phase Behavior of Model Membranes Composed of Phosphatidylcholines Containing Linear Saturated Ijipid, (1987), pp. 6118–6126.
[47] D. Papahadjopoulos, M. Moscarello, E.H. Eylar, T. Isac, Effects of Proteins on Thermotropic Phase Transitions of Phospholipid Mmebranes, 401 (1975), pp. 317–335.
[48] K. Lohner, A. Latal, R.I. Lehrer, T. Ganz, Differential scanning microcalorimetry indicates that human defensin, HNP-2, interacts specifically with biomembrane mimetic systems, Biochemistry 36 (1997) 1525–1531.
[49] E. Sevcsik, G. Pabst, W. Richter, S. Danner, H. Amenitsch, K. Lohner, Interaction of LL-37 with model membrane systems of different complexity: influence of the lipid matrix, Biophys. J. 94 (2008) 4688–4699.
[50] M. Hoernke, C. Schwieger, A. Kerth, A. Blume, Binding of cationic pentapeptides with modified side chain lengths to negatively charged lipid membranes: complex interplay of electrostatic and hydrophobic interactions, Biochim. Biophys. Acta Biomembr. 1818 (2012) 1663–1672.
[51] T. Inoue, Y. Nibu, Phase behavior of hydrated lipid bilayer composed of binary mixture of phospholipids with different head groups, Chem. Phys. Lipids 100 (1999) 139–150.